Design, Fabrication and Analysis of Asymmetric Spiral-arm Mach-Zender Interferometer

YEUNG Tung Yan

Nano-Fabrication, MSc Optoelectronic and Quantum Technologies, Uinversity of Bristol

(Dated: 19 February 2024)

Abstract— An asymmetric spiral-arm Mach-Zehnder Interferometers (MZI) has been designed and fabricated on SOI platform. This research paper presents simulation results that demonstrate the efficient coupling of light of different components within the device. Parameter sweep analysis in fabrication, gap and coupling length of Directional Coupler (DC), arm length difference, and input power highlights the optimized case and showcases the impacts on the effective indices n_{eff}. It is found that Silicon Layer=240nm with etching=110nm of DC has highest n_{eff}. And, the larger the arm length difference, the larger the spread in Frequency Spectrum Range (FSR). Furthermore, this paper reveals the opto-mechnical and thermo-optic (TO) effects within the MZI. Simulation results demonstrate 0.032W is required for this design to induce a π phase shift.

I. INTRODUCTION

Over the last ten years, photonic integrated circuits (PICs) have emerged as a promising solution for inter-chip and intra-chip optical communication. These circuits typically consist of a silicon layer that guides light, positioned on top of a layer of silica known as silicon on insulator (SOI). SOI is particularly advantageous due to two main characteristics: its high refractive index contrast and compatibility with complementary metal-oxide-semiconductor (CMOS) technology. The high refractive index contrast that is between a Si waveguide core and a SiO2 cladding leads to effective confinement of light, facilitating the development of high integration density, compact devices.[1] The state-of-the-art CMOS fabrication techniques guarantee fabrication quality and reliability, which is a major factor in expansion in this field. As a result, photonic devices can now be produced in large quantities and are compatible with integrated circuits (ICs) for electronics.[2] In general, the components of silicon photonic circuits can be divided into active (i.e. laser) and passive (i.e. waveguides, waveguide bends, fiber grating couplers) components. In this paper, an asymmetric MZI built using passive components is studied.

MZI with an emission source around 1550 nm on Silicon-On-Insulator(SOI) platform have proven to be valuable in various applications such as optical switches, filters, modulators, and sensors. This is due to their advantageous characteristics, including high optical index difference, low propagation and coupling losses, as well as a large thermo-optic effect.[3] 1550nm falls within the wavelength range known as the "C band" and is widely used for long-distance transmission in fiber-optic communication

systems. The choice of 1550nm for telecommunications is primarily due to the low attenuation (transmission loss) in optical fibers at this wavelength, which allows for the transmission of signals over long distances without significant degradation. Additionally, 1550nm is less affected by various sources of signal impairments, such as dispersion and non-linear effects.[4]

Refractive index tuning can be achieved through opto-mechanical, thermo-optic[5]–[8], and electro-optic methods[9] to introduce tunability in static nanophotonic devices. This paper examines the opto-mechanical and therm-optic methods. Opto-mechanical method is realised by using a variety of different imbalance lengths. Using spiral-arm MZIs is proofed to have a lower switching power compared to straight-arm[10]. Thermo-optical tunability is realised by placing a micro-heater on upper arm of the MZI. This feature allows control over the transmission properties at desired wavelengths, allowing the achievement of both maximum and minimum transmission levels. This paper investigates the micro-heater feature without its fabrication. The geometrical and performance characteristics of every component and fabrication tolerance were examined using coupled mode analysis, DEVICE, FDE, FDTD, HEAT and INTERCONNECT simulation tools. Simulations and graph plotting methods are used to analyse characterisation from the experimental data.

II. DESIGN AND FABRICATION

The chip is fabricated by the research facility CORNERSTONE, Optoelectronics Research Centre (ORC), Southampton. Using Silicon as a platform for photonics, the advantage of reusing the well-established CMOS processing technology can be leveraged. The dimensions pattern at the design of SOI waveguides carried on a bare silicon wafer are the crystalline silicon (Si) layer thickness ($h_{wg} = 220nm \pm 20nm$), Thermal silica (SiO2) Buried OXide (BOX) layer thickness ($h_{box} = 2\mu m \pm 50nm$) acts as barrier preventing the leakage of guided beam into the Si substrate, Si etch depth ($D = 120nm \pm 10nm$), waveguide width ($W = 450nm$), and top SiO2 cladding ($h_{top} = 1\mu m \pm 100nm$) for protection. The cross-section image of the device is shown in Figure 1. The device is designed for single-mode operation at 1550 nm. All of the components are based on TE mode.
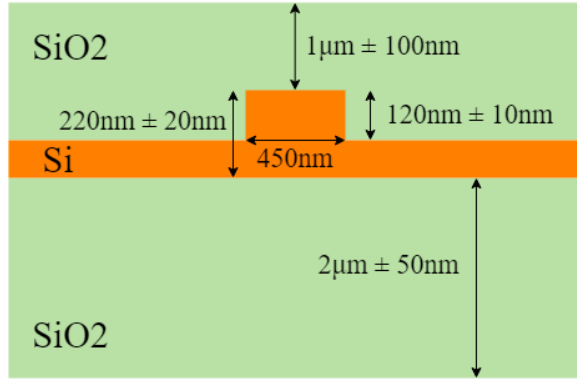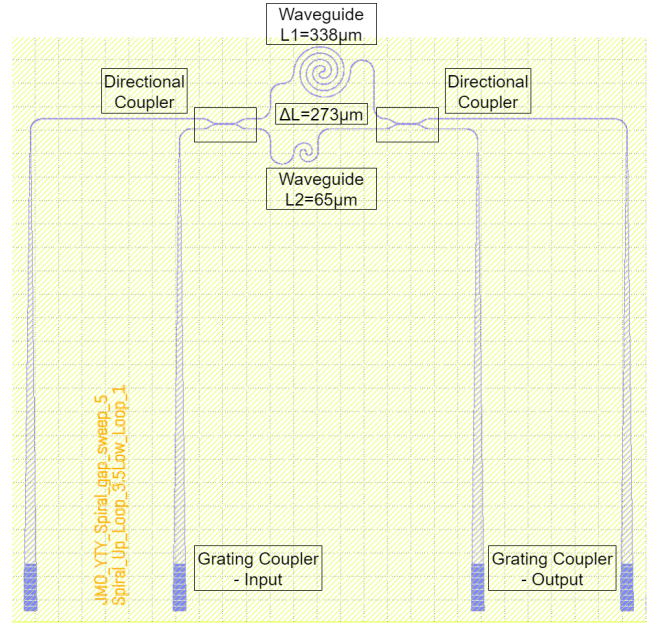
Fig. 1: Dimension of a waveguide.

Fig. 2: GDS layout of a designed MZI.

The fabrication process flow is as follows. Start material is the $220nm$ SOI with $2\mu m$ BOX on a bulk silicon substrate. A resist is firstly spun onto the top surface of the chip. Grating coupler and rib waveguide are patterned via lithography. The chip should then blow-dried and be prepared for the following procedure. Shallow Si etching of $120nm$. The area where the resist was dissolved and removed undergoes etching, while the protected area that protected by the resist remain unetched. This process transfers the patterned resist into the silicon layer of the SOI chip. Subsequently, the remaining resist is removed. The last step is to deposit $1\mu m$ thick SiO2 as top cladding.[11, 12]

The designed MZI device is composed of two grating couplers, two directional couplers and two spirals. Starting from the left grating couplers($10\mu m$ wide tapered to 450nm), the incoming power is split by the first directional coupler into the two arms. Two spiral waveguides which feature a path difference as two ars of the MZI. As the lightwaves propagate through the interferometer, they combine again at the output of the MZI using the second directional coupler. The power transmitted through the second directional coupler is determined by both the amplitudes of the incoming mode and the phase difference between them. A GDS layout of an asymmetric MZI is shown in Figure 2.

III. PHOTONIC COMPONENTS

Waveguides: A waveguide (WG) is a structure designed to confine and guide the propagation of light. The core of the waveguide is composed of Si with a high refractive index of 3.48 at a wavelength of 1550 nm. This high refractive index core is surrounded by SiO2 with a lower refractive index of 1.54 at a wavelength of 1550 nm. This design of low-high-low refractive indices leads to formation of total internal reflection, which is essential for the waveguide to achieving effective light confinement and propagation, as well as protecting the light from escaping into the cladding. The designed device ensures the bending radius in large enough without a noticeable loss to confine light in very compact wire waveguides to create very dense photonic circuits.

The simulated intensity of the E field of the fundamental mode for a waveguide is shown in Figure 3. A mode is a solution to Maxwell's equations that takes boundary conditions and material properties into consideration. It describes the path taken by light across space (or a material). For a fixed geometry, the mode propagates down the waveguide with a constant value .

A plane wave moving in the z-direction has a time-dependent E field that is given as

$$E = E_0 \cdot e^{j(\omega t - \beta z)} \quad (1)$$

using the complex propagation constant β

$$\beta = 2\pi \cdot \frac{n_{eff(\lambda)}}{\lambda} - i \cdot \frac{\alpha}{2} \quad (2)$$

and the radial frequency ω

$$\omega = 2\pi f = \frac{c}{\lambda} \quad (3)$$

The complex propagation constant β explains the variations in phase and amplitude along the propagation direction z while accounting for the effects of dispersion and loss (using the attenuation constantα).[13]

The **refractive index** is the ratio of speed of light in a vacuum to its speed in a certain medium at a given wavelength. λ:

$$n(\lambda, T) = \frac{c}{v(\lambda, T)} \quad (4)$$

In general, the refractive index depends on λ and temperature, the values of refractive index and temperature dependence for Si and SiO2 are given in table I. The themperature dependance $\frac{dn}{dT}$ for Si is high. The thermo-optic effect will be discussed in the later section IV.

The **effective index** n_{eff} is distinct from the refractive index as it accounts for light propagation within a confined structure, like waveguides, where the 2 directions (i.e. x

	Si	SiO_2
Refractive index	3.47	1.44
λ dependence: $\frac{dn}{d\lambda} [nm^{-1}]$	-7.6×10^{-5}	-1.2×10^{-5}
Temperature dependence: $\frac{dn}{dT} [K^{-1}]$	1.87×10^{-4}	8.5×10^{-6}

TABLE I: Properties of the materials Si and SiO2.[14]

and y) are confined. In contrast, there are no constraints in the 3 directions (i.e.x, y, or z) in an unconfined, infinite bulk medium. Simpler to describe, n_{eff} quantifies the phase velocity per unit length in a waveguide relative to the phase velocity in vacuum. Its value depends on the wavelength λ and the specific mode through which the light propagates, which is influenced by the geometry of the waveguide.[15]
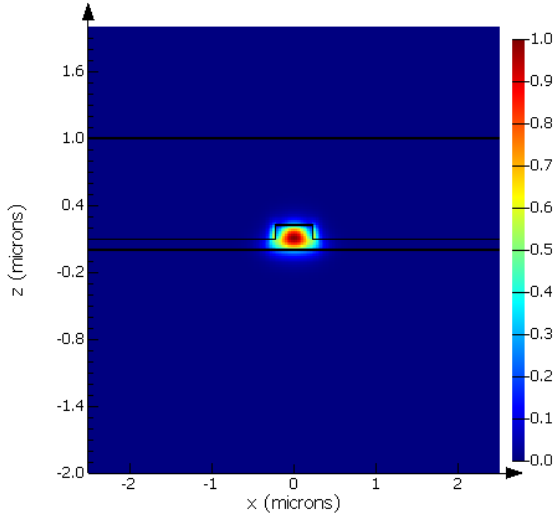

Fig. 3: Simulated TE basic mode profile of standard waveguide.

The **group index** n_g is employed to calculate the free-spectral range (FSR) in MZI. The FSR represents the spacing between adjacent peaks in the effective index versus wavelength. FSR calculation will be mentioned in the later MZI part. It quantifies the shift in the effective index as the wavelength varies:[15]

$$n_g(\lambda) = n_{eff}(\lambda) - \lambda \cdot (\frac{d}{d\lambda} n_{eff}(\lambda)) \qquad (5)$$

The effective index and group index n_g for standard waveguide structure (H = 220nm, HBOX = 2 µm, D = 120 nm, W = 450nm) at 1550 nm is calculated in Mode solution using FDE to be 2.443 and 3.760 respectively. Figure 4 shows the effective index of the standard waveguide against wavelength.

Grating Couplers: A grating coupler consists of a periodic structure, associated with a periodic refractive index, defined in a waveguide. The Bragg condition determines the various angles at which light impinging on the grating will diffract. By placing the single mode fiber 10° with respect to the surface of the chip, we can achieve efficient coupling from the optical fiber into the photonic circuit, and vice versa. The diffraction and thereby the coupling efficiency
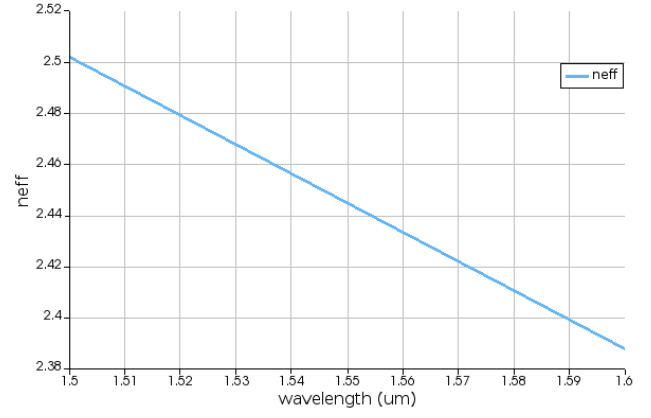
Fig. 4: Effective index of standard waveguide structure.

is very selective to wavelength, propagation direction and polarization. Hence, the grating couplers can only be designed for a specific wavelength and polarization.[16] Grating coupler parameters are as follows, grating taper route = 10 µm, grating coupler width (width of standard waveguide of the device) = 450 nm, period Λ = 670 nm, number of periods = 60, vertical distance (pitch) = 127 µm, fill factor (defined as the ratio of trench width over the period) = 50%, , and taper length = 350 nm. A 2D side view Lumerical simulation model illustrating the input beam from optical fibre coupled into the SOI chip is shown in Figure 5a; Figure 5b shows intensity of the electric field of the grating coupler.

Directional Couplers: Two straight waveguides are placed in close proximity to one another to form the directional coupler, which allows for evanescent field interaction. Both the even and odd modes of the system are activated on the coupling region of a symmetric coupler with identical waveguides, where the coupler mode can be expressed as the superposition of the odd and even modes. The power will cross across waveguides as it travels along the device because the even and odd modes have differing propagation constants, which will cause their relative phases to change as they travel down the coupler.

To calculate the coupling length by taking the index differences between the two coupled modes. The difference in the indices is

$$\Delta n = neff1 - neff2 \qquad (6)$$

Waveguide 1 should have 100% of the power at first, and waveguide 2 should have roughly 50% of the power. By solving for L, determine the coupling length needed to provide 50% power coupling to waveguide 2.
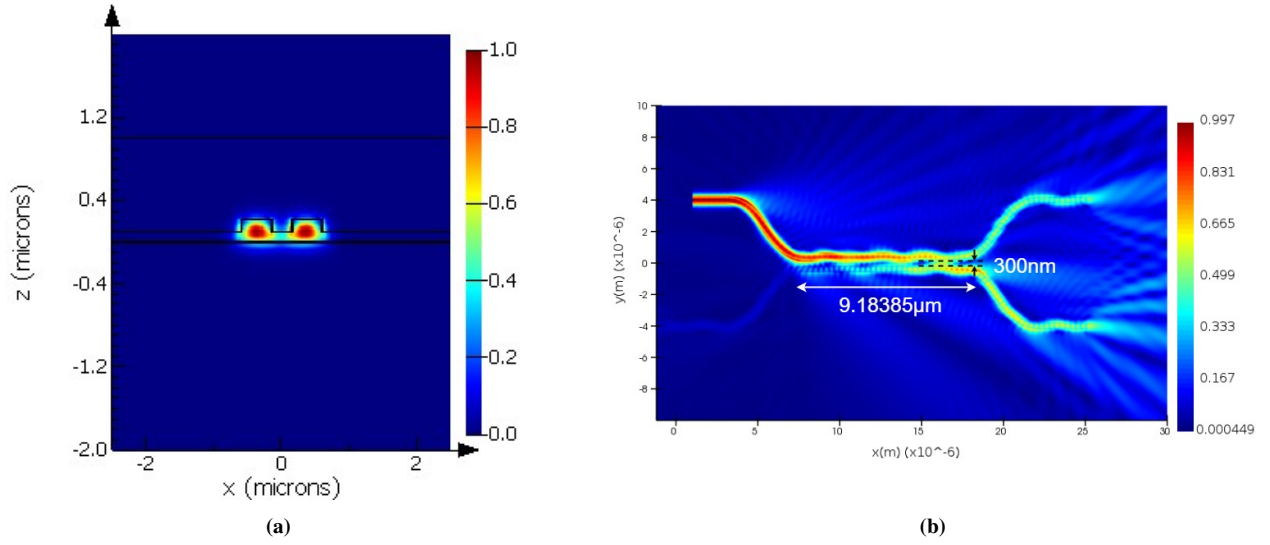
$$L = \frac{\lambda_0}{\pi \Delta n} \sin^{-1}(\sqrt{\frac{P_2}{P_0}}) \qquad (7)$$

Where L is the coupling length, P_0 is the input power, $\frac{P_2}{P_0} = 0.5$, and λ is 1550nm.

The n_{eff1} and n_{eff2} are first calculated in FDE varying the gap from 290 nm to 310 nm. Figure6a shows the
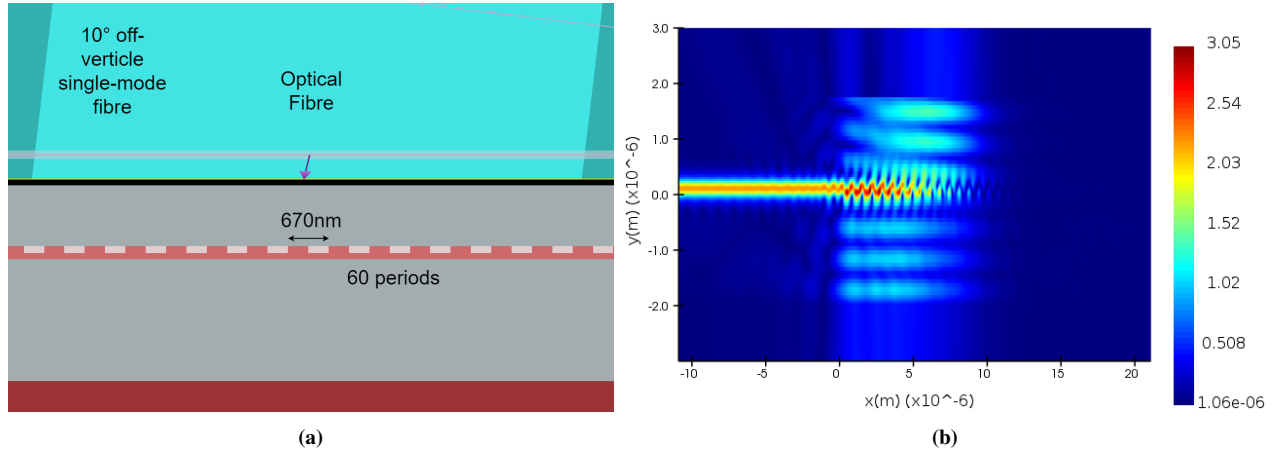
Fig. 5: (a) Grating Coupler coupling to integrated waveguides with from a near-vertical single-mode fiber. (b) Simulated E-field Intensity of the designed Grating Coupler.

Fig. 6: (a) Simulated TE basic mode profile of Directional Coupler with gap = 0.3um. (b) Simulated E-field Intensity of the Directional Coupler with gap=300nm and length=9.18385μm.

TE mode profile of the DC with gap = 0.3 μm. The values are then used to calculate the coupling length by equation (5). Lastly, create a DC in Lumerical MODE and input the calculated coupling gap and length, use FDTD to generate the electric field intensity profile. The generated Figure6b displays the distribution of the electric field on a symmetric DC with gap=300nm and length=9.18385μm. The DC parameter is randomly chosen from Table II to simulate a demonstration for E field profile. An almost 50% 50% splitting ratio is observed. The observed discrepancy between the theoretical calculations and the simulation results in the case of the directional coupler can be because of material properties and numerical approximation. Since the simulation processes included different softwares in different stages, the properties of the materials may have slight variations from their nominal values. Apart from this, the simulation in Lumerical relies on numerical methods and approximations to solve the underlying equations. These approximations may introduce small errors that accumulate and affect the

simulation results.

A higher effective index is desirable in waveguides because it enables better light confinement and tighter mode confinement, leading to improved light propagation characteristics such as reduced mode dispersion, increased waveguide bandwidth. By doing sweep experiment using FDE method, Figure 7c shows etch with 110nm has highest n_{eff}. Using etch 110nm, sweep the Si layer thickness with 200nm, 220nm and 240nm. Neff values with 110nm etch and 240nm Si layer thickness is highest. The results show the fabrication thickness impact to DC. The sweep DC data is plotted in Figure 7a - 7d and listed in Table II - III.

Mach-Zehnder interferometers: The MZI is a device that splits optical power into two arms and then recombines it into a single waveguide. By utilizing opto-mechanical techniques, the phase of the light can be altered in one or both arms. This can be achieved by introducing a difference in the optical path length or by modulating the refractive index. As a result,
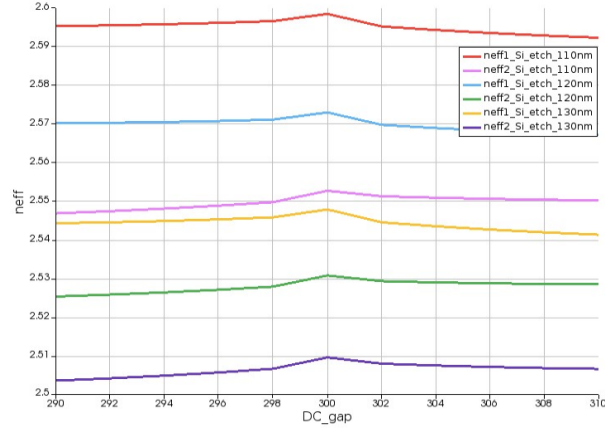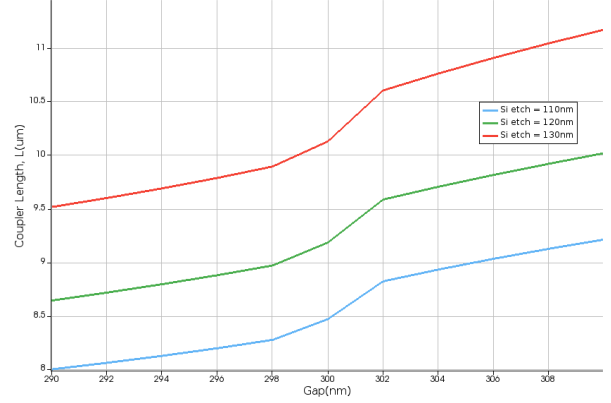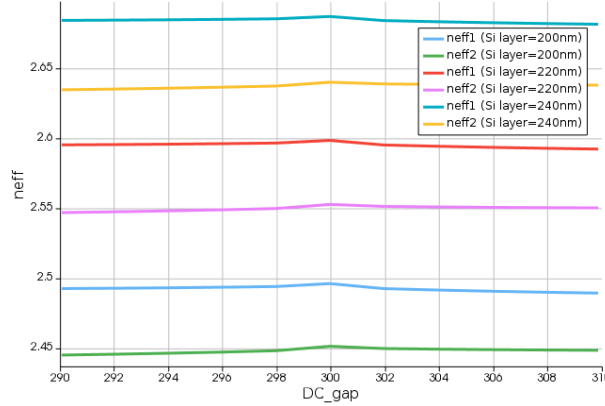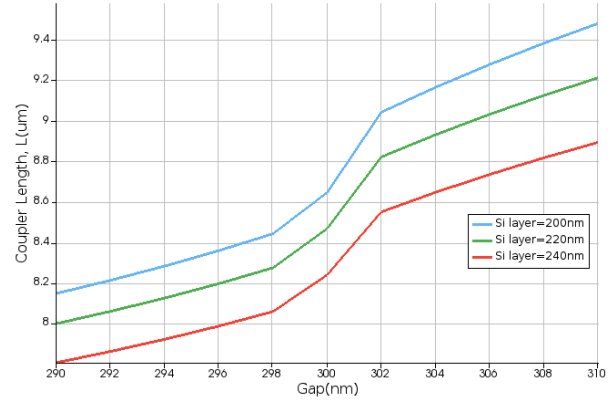
Fig. 7: (a) Neff vs DC gap (nm) sweeping etch depth with fixed Si layer h_{wg}=220nm. (b) DC length (um) vs DC Gap (nm) sweeping etch depth with fixed Si layer h_{wg}=220nm. (c) Neff vs DC gap (nm) sweeping Si layer h_{wg} with fixed etch depth D=110nm. (d) DC length (um) vs DC Gap (nm) with Si layer h_{wg} sweeping Si layer h_{wg} with fixed etch depth D=110nm.

DC Gap (nm)	Si etch 110nm			Si etch 120nm			Si etch 130nm		
	neff1	neff2	DC length	neff1	neff2	DC length	neff1	neff2	DC length
290	2.59526	2.54682	8.00077	2.57015	2.52532	8.64282	2.54428	2.50356	9.51536
292	2.59546	2.54739	8.06135	2.57026	2.5258	8.71683	2.54452	2.50415	9.59918
294	2.59573	2.54805	8.12666	2.57044	2.52638	8.79518	2.54484	2.50485	9.68919
296	2.59609	2.54882	8.19771	2.57071	2.52706	8.87897	2.54526	2.50567	9.78667
298	2.59655	2.54973	8.27584	2.57108	2.52788	8.96971	2.5458	2.50663	9.89328
300	2.59842	2.55267	8.46914	2.57294	2.53074	9.18385	2.54782	2.50956	10.1274
302	2.59517	2.55124	8.82197	2.56972	2.52929	9.58502	2.54449	2.50795	10.6029
304	2.59425	2.55086	8.93131	2.5689292	2.52896	9.70395	2.54348	2.50747	10.7604
306	2.59347	2.55057	9.03193	2.56821	2.52873	9.81454	2.54263	2.5071	10.9063
308	2.59281	2.55034	9.12509	2.56764	2.52857	9.91854	2.5419	2.50681	11.0422
310	2.59225	2.55018	9.21182	2.56716	2.52847	10.0173	2.54129	2.5066	11.1694

TABLE II: DC sweep data with fixed Si layer h_{wg}=220nm.

DC Gap (nm)	$h_{wg} = 200nm$			$h_{wg} = 220nm$			$h_{wg} = 240nm$		
	neff1	neff2	DC length	neff1	neff2	DC length	neff1	neff2	DC length
290	2.49251	2.44495	8.14921	2.59526	2.54682	8.00077	2.68425	2.63462	7.80828
292	2.49273	2.44556	8.21428	2.59546	2.54739	8.06135	2.68443	2.63515	7.86369
294	2.49304	2.44627	8.28429	2.59573	2.54805	8.12666	2.68467	2.63577	7.92351
296	2.49345	2.4471	8.36031	2.59609	2.54882	8.19771	2.68499	2.63648	7.98869
298	2.49396	2.44807	8.44374	2.59655	2.54973	8.27584	2.68538	2.63731	8.06043
300	2.49604	2.45122	8.6467	2.59842	2.55267	8.46914	2.68705	2.64003	8.24114
302	2.49247	2.44962	9.04254	2.59517	2.55124	8.82197	2.68411	2.63879	8.55127
304	2.49146	2.44918	9.16494	2.59425	2.55086	8.93131	2.68329	2.63848	8.64752
306	2.4906	2.44883	9.27771	2.59347	2.55057	9.03193	2.68259	2.63823	8.73599
308	2.48987	2.44857	9.38223	2.59281	2.55034	9.12509	2.68199	2.63804	8.81783
310	2.48925	2.44838	9.47961	2.59225	2.55018	9.21182	2.68148	2.63791	8.89397

TABLE III: DC sweep data with fixed Si etch depth D=110nm.

the MZI functions as an interferometer, capable of converting phase changes into intensity changes.[17]

An asymmetric MZI, can also function as a wavelength filter in situations when one of the arms is longer than the other. In the literature review, this behaviour is governed by these equations:[18]

$$\eta = \frac{P_{out}}{P_{in}} = cos^2(\frac{\Delta\phi}{2}) \qquad (8)$$

$$\Delta\phi = \frac{2\pi\eta_{eff}\Delta L}{\pi} \qquad (9)$$

Where η is the Mach-Zehnder efficiency, P_{out} is the output power, P_{in} is the input power, $\Delta\phi$ is the phase change, ΔL is the length differences of the two arms. In the ideal case, when a π phase shift is introduced, the extinction ratio $P_\eta = 0/P_\eta = 1$ is expected to be 0. However, the extinction ratio can be compromised due to optical absorption occurring within each arm of the MZI.

The transfer function for a lossless, asymmetric interferometer is given as

$$\frac{I_{out}}{I_{in}} = \frac{1}{2}[1 + cos(\beta \cdot \Delta L)] \qquad (10)$$

assuming $L_1 \neq L_2$ and the propagation constants $\beta_1 = \beta_2$. The output intensity (in dB) is given as[19]

$$I_{out} = 10 \cdot log_{10}(|E_{out}^2|) \qquad (11)$$

When there is a disparity in length between the arms of the Mach-Zehnder Interferometer (MZI), it introduces an extra phase shift in one of the arms. This discrepancy leads to a periodic transfer function in relation to the wavelength λ. This periodicity is referred to as the FSR and is estimated by first order approximation of dispersion using[20]

$$FSR = \Delta\lambda = \lambda_{m+1} - \lambda_m \approx \frac{\lambda^2}{\Delta L \cdot n_g(\lambda)} \qquad (12)$$

The sweep data in the arm lengths is listed in Table IV.

	L1	L2	ΔL
Design TE #0	65	65	0
Design TE #1	103	65	38
Design TE #2	149	65	84
Design TE #3	203	65	138
Design TE #4	266	65	201
Design TE #5	338	65	273
Design TE #6	418	65	353

TABLE IV: Arm difference sweep data. (in μm)

The waveguide properties, such as n_{eff}, n_g, and dispersion are obtained from Lumerical Mode Calculation. In these simulations, both waveguides are modeled with identical geometries and material properties. The only difference between the two waveguides is their lengths. The above calculated properties is then imported and implement simulation in INTERCONNECT to show the transmission spectrum and FSR with some of the designed arm length sweep. The following Figure 8 - 9 summarize the results. The experimental results indicate that the spread in FSR
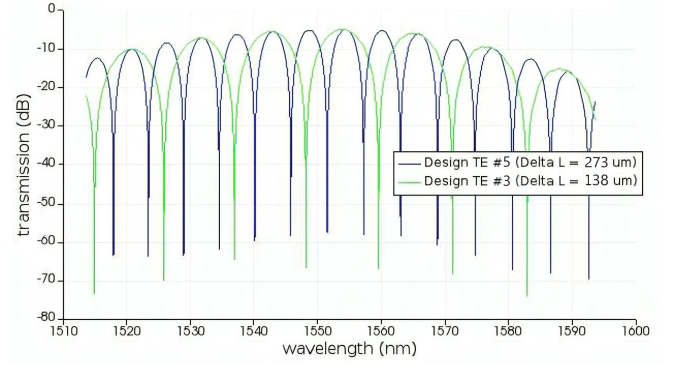
Fig. 8: Simulated results of Transmission vs Wavelength.
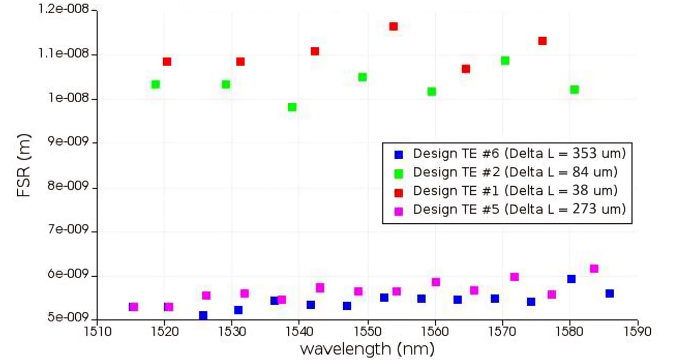
Fig. 9: Simulated results of FSR vs Wavelength.

increases when ΔL (i.e. 38 μm) drops, but FSR lowers with an increasing ΔL (i.e. 353 μm). It demonstrates an inversely proportional relationship of the spread of FSR and ΔL. Also, the FSR increases for decreasing group index n_g and imbalance length ΔL, whereas it will increase for increasing wavelengths.

IV. DISCUSSION

Apart from exploiting refractive index tuning through opto-mechanical method, therm-optic method is widely used. In the session, how thermo-optic effect induce phase shift will be discussed.

Due to large thermo-optic effect of Si, the real part of the refractive index of the material might vary depending on the temperature of the material.Refer to the Table I in Section II, since $\frac{dn}{dT}$ for Si is considerably higher than that of SiO2, the effective index shift of the Si wire waveguide and the temperature shift in Si refractive index are equal.

Literature reviews show the common fabrication of the thermo-optics phase shifter. Overhead heater design is selected in this research work.

A heater is positioned above the silicon waveguide, which is patterned right on top of the original SiO2 cladding. It is mentioned that in order to prevent significant optical insertion loss, the vertical separation between the heater and waveguide should be maintained at a large enough size. For this project, the original cladding gap is large enough.[6,7] The materials that can be used for an overhead heater are restricted to those that are in the fabrication at the

relevant point of the process flow.Nevertheless, the majority of these materials are employed as diffusion barrier thin films, and the processes may not always be capable to deposit thick enough patterned heater lines. Resistivity and melting point of tungsten (8 $\mu\Omega$-cm and 3417 ℃ respectively) are higher than that of copper (1.68 $\mu\Omega$-cm and 1083 ℃ respectively), implying that tungsten heater can be used at higher temperatures and also require less driving current to reach a given amount of power dissipation.[8] Therefore, tungsten is chosen to be the overhead heater material.

In the DEVICE project, we first place a wire 2um above the waveguide and acts as a heat source. The overhead tungsten heater for thermo-optic tuning is shown in 10a. The heat source is used to tune the waveguide and achieve the desired phase shift. Using the HEAT, we then sweep the input power in a balanced MZI and obtain the temperature profile at the waveguide cross-section for different input power values. Using the FDE, we obtain the temperature-dependent effective index of the waveguide's fundamental mode by sweeping the input power and calculate the corresponding phase shift.The local heat generated by the microheaters when a voltage is applied causes a phase change in the MZI arm. Figure 10b shows 0.032W is required to induce a phase

shift of π. Figure 10c - 10d demonstrate the temperature profile simulated by HEAT showing the temperature variation under different input power. Due to the software simulation limitation, only the thermo-optic effects of straight arm waveguide can be realised. But through literature review, it demonstrates employing spiral-arm MZIs results in lower switching power when compared to straight arms due to the intense heat concentration in the center of spiral.[21]

V. CONCLUSIONS

To summarise, an aMZI structure using the popular SOI technology have been proposed. The parameter sweeps performed in Silicon Layer thickness and Etching thickness along with DC gap and coupling length have demonstrated the fabrication tolerances and the changes in effective indices. Four of the designs for optical filters with different FSR were implemented and characterized both experimentally and graphically. The analysis demonstrates relatinoship between the ΔL and the spread in FSR, as well as n_g and ΔL. Aside from the above imbalanced arm opto-mechanical effects found in MZI, the balanced arm thermo-optic fabrication and effect have been examined. A tunsten overhead heater is applied and proofed an input power of 0.032W can cause a π phase shift.
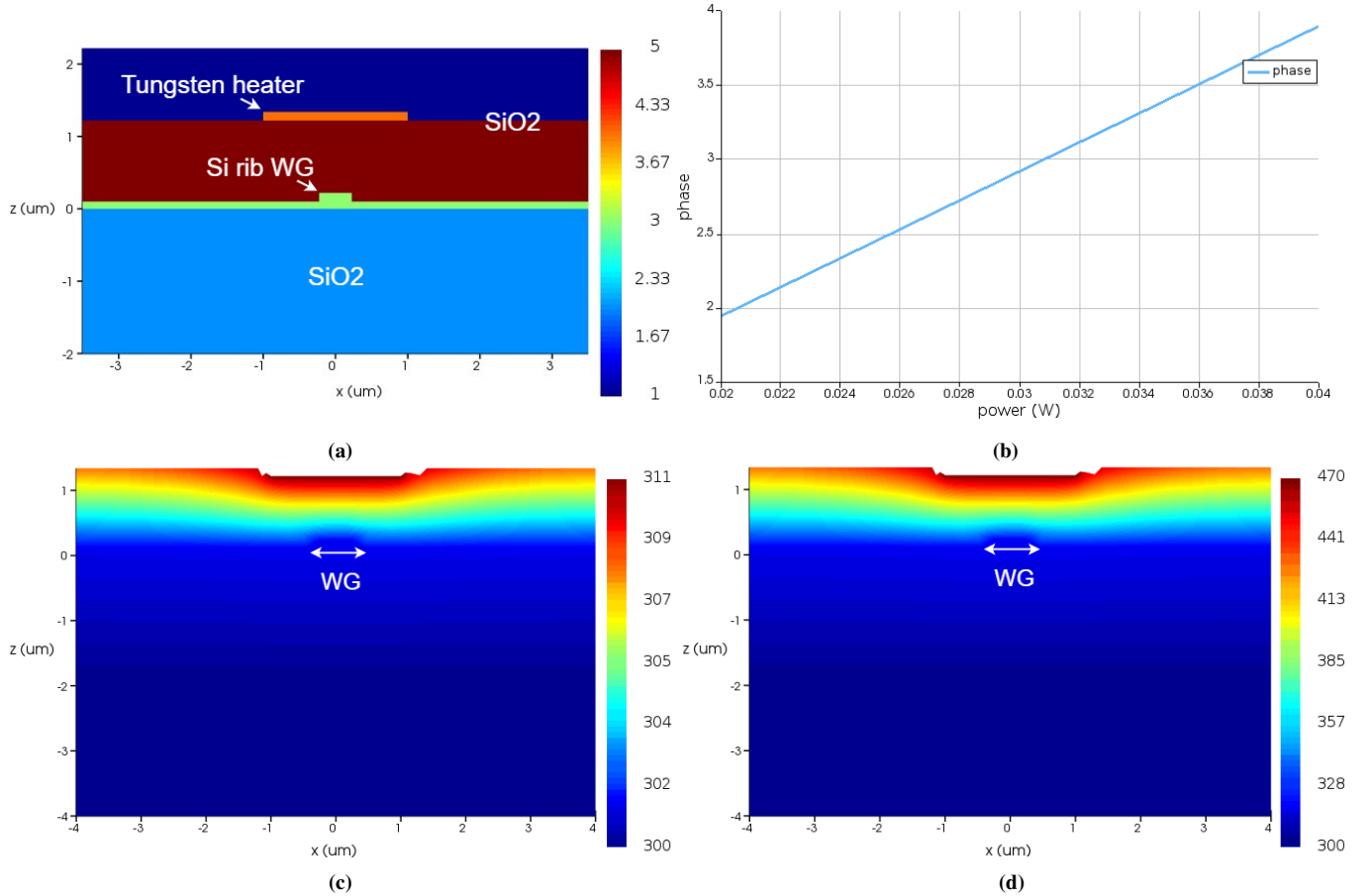
Fig. 10: (a) Labelled schematic cross-section diagram of thermo-optic phase shifters, with metal heaters. (b) Phase vs Input Power (W) with balanced arm length and heating the upper arm of MZI. (c) Temperature profile with applying 0.032W. (d) Temperature profile with applying 0.5W.

References

[1] R. Baets, A. Z. Subramanian, S. Clemmen, B. Kuyken, P. Bienstman, N. Le Thomas, G. Roelkens, D. Van Thourhout, P. Helin, and S. Severi, "Silicon photonics: Silicon nitride versus silicon-on-insulator," pp. 1–3, 2016.

[2] Q. Teng, Y. Hu, R. Cheng, Y. Wu, G. Zhou, and D. Gao, "Reliability challenges in cmos technology: A manufacturing process perspective," tech. rep., 2023.

[3] C. Rizal and B. Niraula, "Compact si-based asymmetric mzi waveguide on soi as a thermo-optical switch," vol. 410, pp. 947–955, 2018.

[4] A. Docherty, "Collision induced timing shifts in wavelength-division-multiplexed optical fiber communications systems,"

[5]

[6] B. Pant, W. Zhang, M. Ebert, X. Yan, H. Du, M. Banakar, D. T. Tran, Y. Qi, D. Rowe, V. Jeyaselvan, C. G. Littlejohns, G. T. Reed, and D. J. Thomson, "Study into the spread of heat from thermo-optic silicon photonic elements," *Opt. Express*, vol. 29, pp. 36461–36468, Oct 2021.

[7] S. Liu, J. Feng, y. Tian, H. Zhao, L. Jin, B. Ouyang, J. Zhu, and J. Guo, "Thermo-optic phase shifters based on silicon-on-insulator platform: state-of-the-art and a review," vol. 15, 12 2022.

[8] A. Masood, M. Pantouvaki, D. Goossens, G. Lepage, P. Verheyen, J. V. Campenhout, P. P. Absil, D. V. Thourhout, and W. Bogaerts, "Fabrication and characterization of cmos-compatible integrated tungsten heaters for thermo-optic tuning in silicon photonics devices," *Optical Materials Express*, vol. 4, pp. 1383–1388, 2014.

[9] S. Kaur, M. Singh, Priyanka, H. Singh, and M. L. Singh, "Design and performance analysis of 2x2 electro-optic based mzi switch using ti:linbo3 as a waveguide at 1.46μm," in *2019 IEEE International Conference on Electrical, Computer and Communication Technologies (ICECCT)*, pp. 1–5, 2019.

[10] M. Nedeljkovic, S. Stanković, C. J. Mitchell, A. Z. Khokhar, S. A. Reynolds, D. J. Thomson, F. Y. Gardes, C. G. Littlejohns, G. T. Reed, and G. Z. Mashanovich, "Mid-infrared thermo-optic modulators in soi," *IEEE Photonics Technology Letters*, vol. 26, no. 13, pp. 1352–1355, 2014.

[11] A. Liu, H. Rong, R. Jones, O. Cohen, D. Hak, and M. Paniccia, "Optical amplification and lasing by stimulated raman scattering in silicon waveguides," *Lightwave Technology, Journal of*, vol. 24, pp. 1440 – 1455, 04 2006.

[12] C. Alonso-Ramos, A. O.-M. nux, I. Molina-Fernández, P. Cheben, L. Zavargo-Peche, and R. Halir, "Efficient fiber-to-chip grating coupler for micrometric soi rib waveguides," *Opt. Express*, vol. 18, pp. 15189–15200, Jul 2010.

[13] R. Sobot, *Introduction*, pp. 1–29. Boston, MA: Springer US, 2012.

[14] J. Low, M. Kreider, D. Pulsifer, A. Jones, and T. Gilani, "Band gap energy in silicon," *American Journal of Undergraduate Research*, vol. 7, 06 2008.

[15] W. J. Westerveld and H. P. Urbach, "Waveguides," in *Silicon Photonics*, 2053-2563, pp. 2–1 to 2–36, IOP Publishing, 2017.

[16] R. Marchetti, C. Lacava, L. Carroll, K. Gradkowski, and P. Minzioni, "Coupling strategies for silicon photonics integrated chips," *Photon. Res.*, vol. 7, pp. 201–239, Feb 2019.

[17] M. Kitsara, K. Misiakos, I. Raptis, and E. Makarona, "Integrated optical frequency-resolved mach-zehnder interferometers for label-free affinity sensing," *Opt. Express*, vol. 18, pp. 8193–8206, Apr 2010.

[18] L. A. Bui, H. Chen, and E. H. W. Chan, "Wavelength switching technique for phase interrogation of mach zehnder interferometer-based optical sensors," *Opt. Express*, vol. 31, pp. 43560–43573, Dec 2023.

[19] S. Marrujo-García, I. Hernández-Romano, D. A. May-Arrioja, V. P. Minkovich, and M. Torres-Cisneros, "In-line mach–zehnder interferometers based on a capillary hollow-core fiber using vernier effect for a highly sensitive temperature sensor," *Sensors*, vol. 21, p. 5471, Aug. 2021.

[20] C. J. Oton, C. Manganelli, F. Bontempi, M. Fournier, D. Fowler, and C. Kopp, "Silicon photonic waveguide metrology using mach-zehnder interferometers," *Optics Express*, vol. 24, p. 6265, Mar. 2016.

[21] A. P. Ovvyan, N. Gruhler, S. Ferrari, and W. H. P. Pernice, "Cascaded mach–zehnder interferometer tunable filters," *Journal of Optics*, vol. 18, p. 064011, May 2016.

VI. Appendix

Source codes for generating GDSII, generated GDSII layout, and Lumerical Simulation projects for each component are available at `https:\github.com/ansontyyeung/MScNanoFab`.

Please refer to the comments in $GDS/design\_space.py$ to check the details of parameter sweep.

Only projects below 100MB are uploaded.